Electronic Supplementary Information

Experimental section

Materials: Sodium Tungstate Dihydrate ($Na_2WO_4·2H_2O$), Nickel foam (NF), Nickel chloride hexahydrate ($NiCl_2·6H_2O$), acetone (C_3H_6O), anhydrous ethanol (C_2H_6O), ammonium chloride (NH_4Cl), sodium hydroxide (NaOH), salicylic acid ($C_7H_6O_3$), sodium citrate dihydrate ($C_6H_5Na_3O_7·2H_2O$), p–dimethylaminobenzaldehyde ($C_9H_{11}NO$), and sodium nitroferricyanide dihydrate ($C_5FeN_6Na_2O·2H_2O$) were purchased from Chengdu Kelong Ltd.

Preparation of C-$NiWO_4$: Typically, 2.3 g of $Na_2WO_4·2H_2O$ and 1.66 g of $NiCl_2·6H_2O$ were dissolved in 70 mL of deionized water, respectively, and then mixed with slow stirring for one hour. Finally, the product was transferred to a 100 ml sealed Teflon-lined stainless steel autoclave. Subsequently, the Nickel foam (NF) was ultrasonically cleaned with acetone, ethanol, and deionized water for 10 min and dried in air. And, the cleaned NF was placed in the solution in an autoclave. Then the autoclave was kept at 160 °C for 6 h. After the autoclave cooled down at room temperature, the NF was taken out, washed with water and ethanol several times, and subsequently dried at 60 ºC overnight.

Preparation of N-$NiWO_4$: 0.33 g of $Na_2WO_4·2H_2O$ and 1.66 g of $Ni(NO_3)_2·6H_2O$ were dissolved in 40 mL of deionized water, respectively, and then mixed with slow stirring for one hour. Finally, the product was transferred to a 50 ml sealed Teflon-lined stainless steel autoclave. Subsequently, the Nickel foam (NF) was ultrasonically cleaned with acetone, ethanol, and deionized water for 10 min and dried in air. And, the cleaned NF was placed in the solution in an autoclave. Then the autoclave was kept at 180 °C for 8 h. After the autoclave cooled down at room temperature, the NF

was taken out, washed with water and ethanol several times, and subsequently dried at 60 ºC overnight.

Characterizations: The crystal structure of the prepared material was determined using an X-ray diffractometer with Cu Kα radiation (DX-2700B). microstructural observations were performed on a field−emission scanning electron microscopy (FEI Insect F50) and an atomic resolution scanning transmission electron microscopy (FEI Talos F200S Super). XPS measurements were carried out with Thermo Fischer ESCALAB Xi^+. The absorbance data were measured via an Ultraviolet-visible (UV–Vis) spectrophotometer (Shimazu UV–2600). EPR spectrum was recorded on a Brüker EMX spectrometer at room temperature.

Electrochemical measurements: All electrochemical measurements were carried out in an H−shaped electrochemical cell separated by Nafion 117 membrane using CHI 760E electrochemical workstation (Chenhua, Shanghai). The area of the working electrode immersed in the electrolyte is 0.25 cm^2. LSV was performed in Ar−saturated 0.1 M NaOH with 0.1 M $NaNO_2$ at a scan rate of 5 mV s^{-1}. All potentials reported in this work were converted to a reversible hydrogen electrode (RHE) scale, and current densities were normalized to the geometric surface area. All experiments were carried out at room temperature (25 °C).

Determination of NH_3: The NH_3 concentration in the electrolyte was determined (the obtained electrolyte was diluted 50 times) by the indophenol blue method. Specifically, 2 mL of electrolyte collected after electrolysis was mixed with 2 mL of coloring solution (1 M NaOH containing 5% salicylic acid and 5% sodium citrate), and 1 mL of oxidizing solution (0.05 M NaClO). Then 0.2 mL oxidation solution

(0.05 M NaClO) mL catalyst solution (1 wt% $C_5FeN_6Na_2O\ 2H_2O$) was dropped into the collected solution. After standing in the dark for 2 h, the concentration of NH_3 was determined by UV-Vis at a specific wavelength of 655 nm. The concentration−absorbance curve was calibrated using the standard NH_4Cl solution with known concentrations of 0.0, 0.25, 0.5, 1.0, 1.5, 2.0, and 2.5 μg mL^{-1} in 0.1 M NaOH. The fitting curve ($y = 0.45557x + 0.02848$, $R^2 = 0.9999$) shows good linear relation of absorbance value with NH_3 concentration.

Determination of NH_3 yield and FE:

The NH_3 FE is estimated from the charge consumed for NO_2^- reduction and the total charge passed through the electrode:

$$FE = 6 \times F \times V \times [NH_3] / (Q \times 17) \times 100\%$$

The yield rate of NH_3 (aq) is calculated:

$$NH_3\ yield = V \times [NH_3] / (A \times t \times 17)$$

Where $[NH_3]$ is the concentration of NH_3 (aq), F is the Faradaic constant (96485 C mol^{-1}), V is the volume of electrolyte in the anode compartment (45 mL), Q is the total charge passing the electrode, t is the electrolysis time, and A is the geometric surface area.

DFT calculation details: Spin-polarized density functional theory (DFT) calculations within Perdew-Burke-Ernzerhof (PBE) generalized gradient approximation (GGA) functional were performed in the VASP package.[1-3] The interaction between valence electrons and the ionic core was expanded using the projector augmented wave (PAW).[4] The DFT-D3 semi-empirical correction was adopted to calibrate van der

Waals forces.[5] The DFT+U approach with U – J = 6 eV for both of Ni and W was employed.[6] $NiWO_4$(002) slab models with a vacuum region thickness of 15 Å were built. The cutoff energy is 450 eV, and the Brillouin zone was sampled in a 3×2×1 mesh. The force convergence thresholds are 0.02 eV/Å, and the total energy is less than 1E-5 eV, respectively.

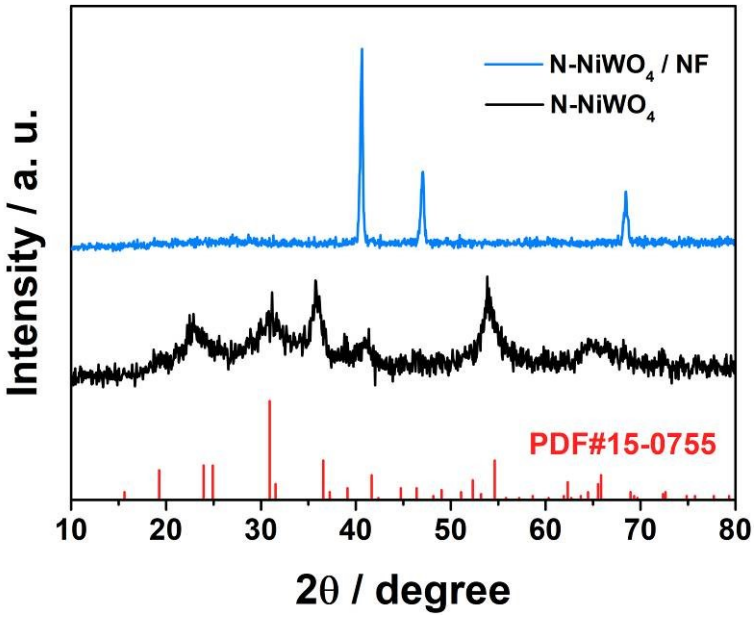

Fig. S1. XRD pattern of the N-$NiWO_4$.

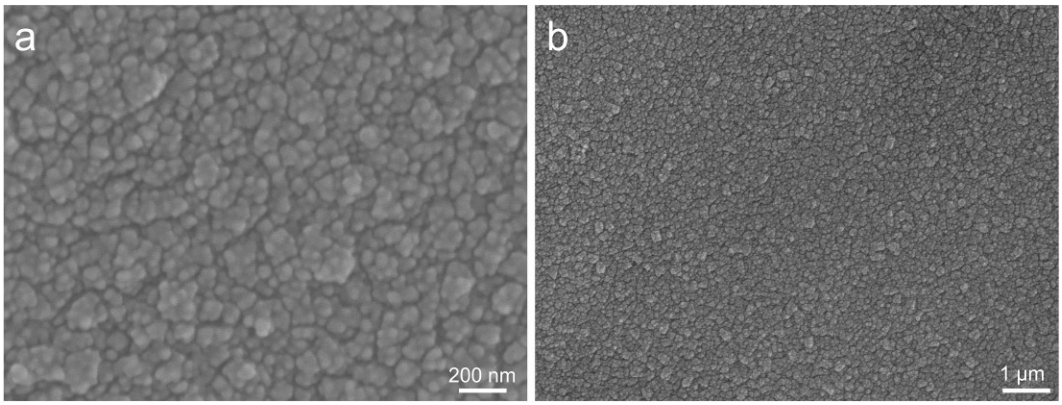

Fig. S2. SEM images of the N-$NiWO_4$/NF.

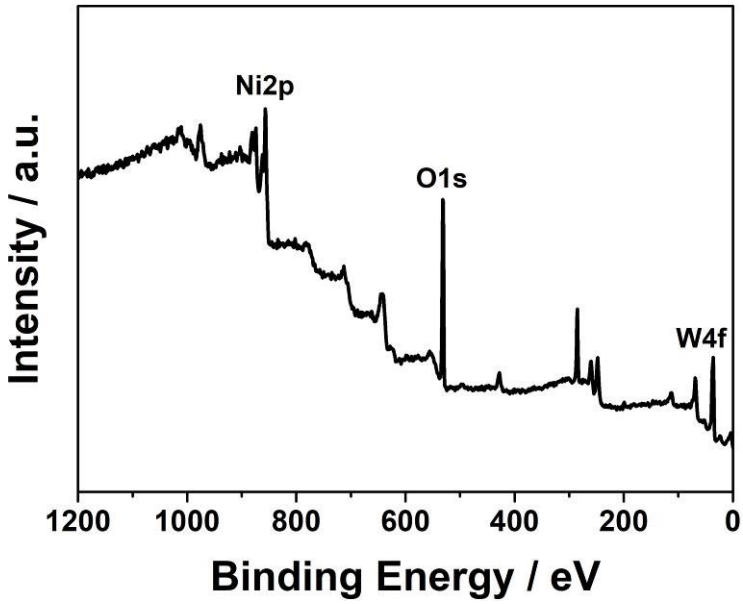

Fig. S3. XPS survey spectrum of C-$NiWO_4$/NF.

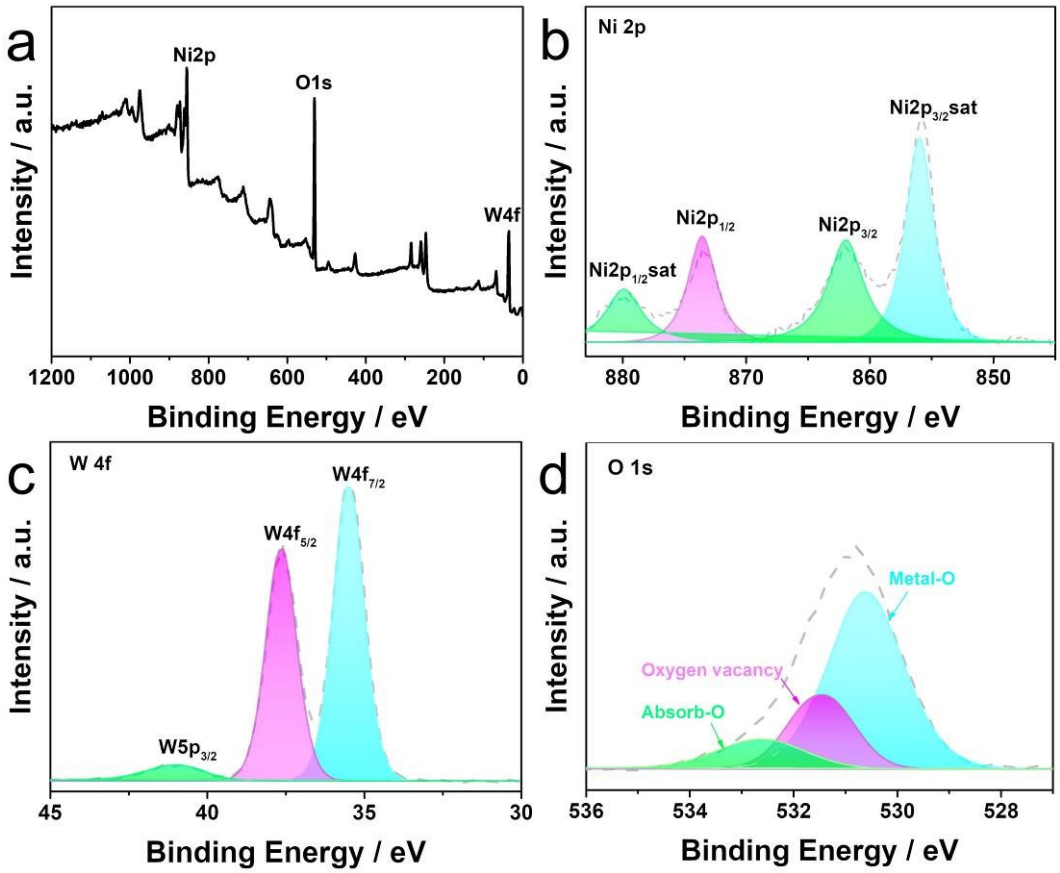

Fig. S4. (a) XPS survey spectrum of N-$NiWO_4$/NF. High-resolution XPS spectra of Ni 2p (b), W 4f (c) and O 1s (d).

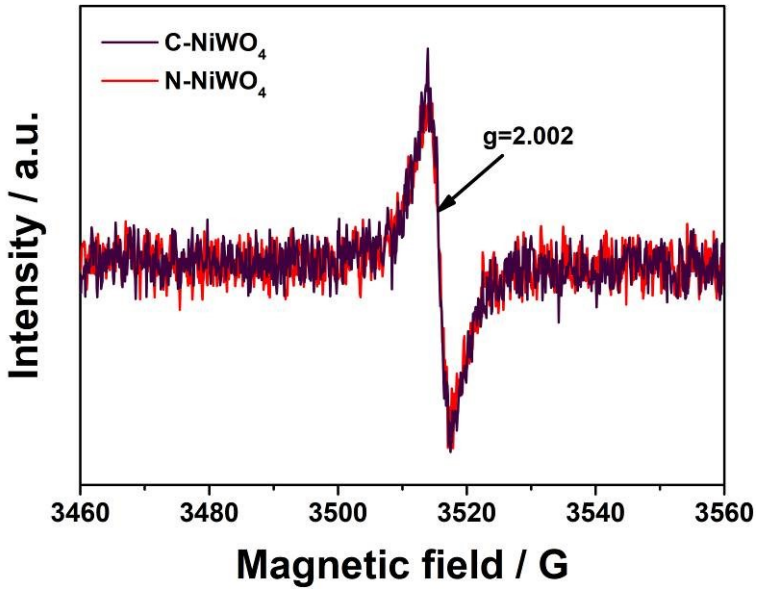

Fig. S5. EPR spectra of C(N)-$NiWO_4$/NF.

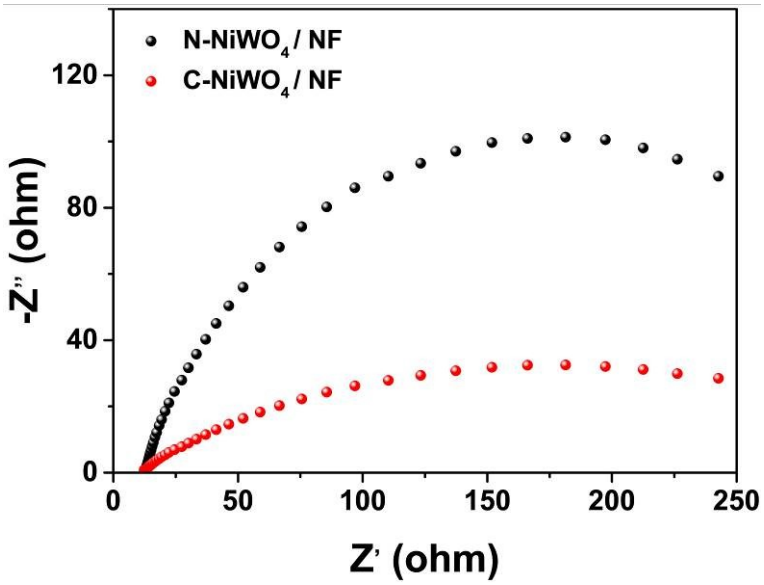

Fig. S6. Nyquist plots for C-$NiWO_4$/NF and N-$NiWO_4$/NF.

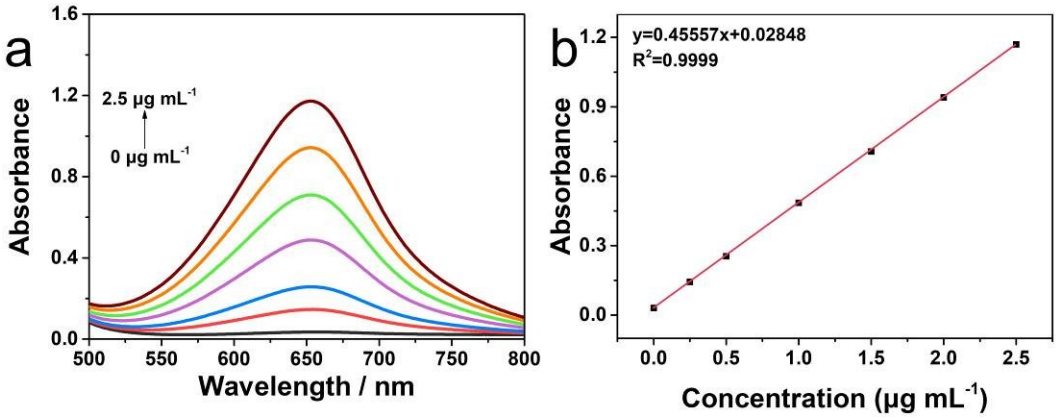

Fig. S7. (a) UV−Vis spectra and (b) corresponding calibration curves were used to calculate NH_4^+.

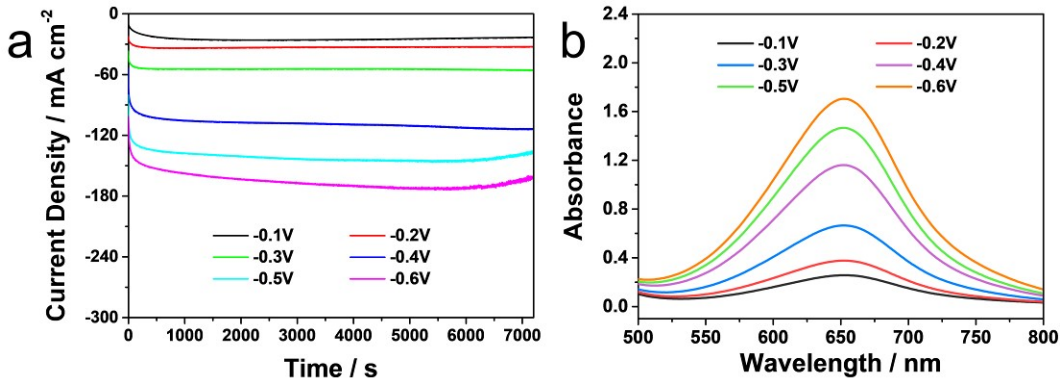

Fig. S8. (a) Chronoamperometry curves and (b) corresponding UV-Vis spectra of C-$NiWO_4$/NF from -0.1 V to -0.6 V.

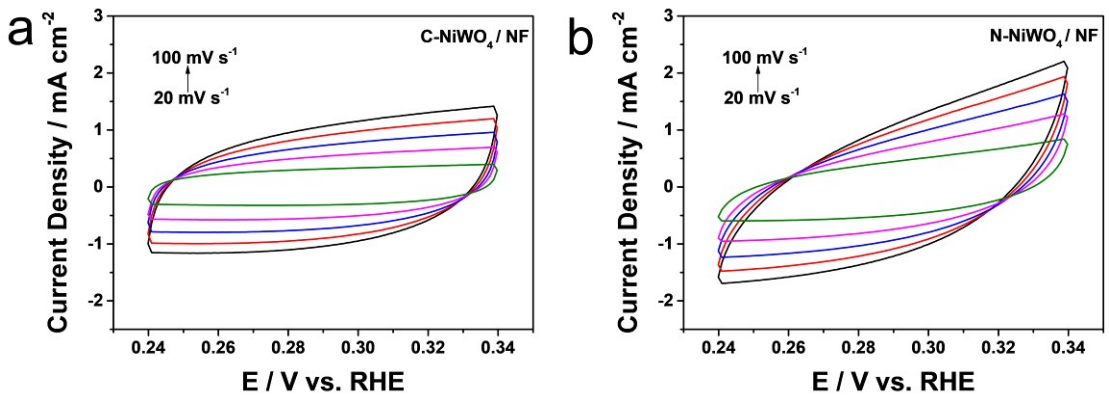

Fig. S9. CV curves of C-$NiWO_4$/NF (a), N-$NiWO_4$/NF (b) at different scan rates (20-100 mV s^{-1})

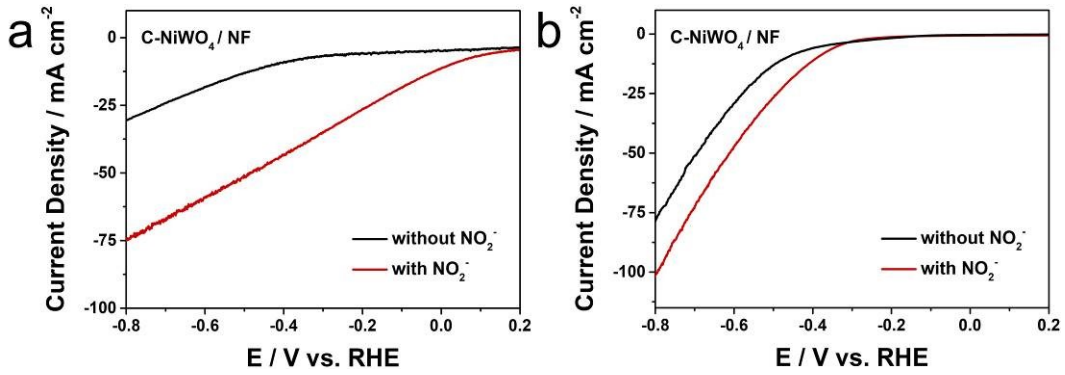

Fig. S10. (a) LSV curves of C-$NiWO_4$/NF in 0.1 M PBS with and without 0.1 M NO_2^- and (b) LSV curves of C-$NiWO_4$/NF in 0.5 M Na_2SO_4 with and without 0.1 M NO_2^-.

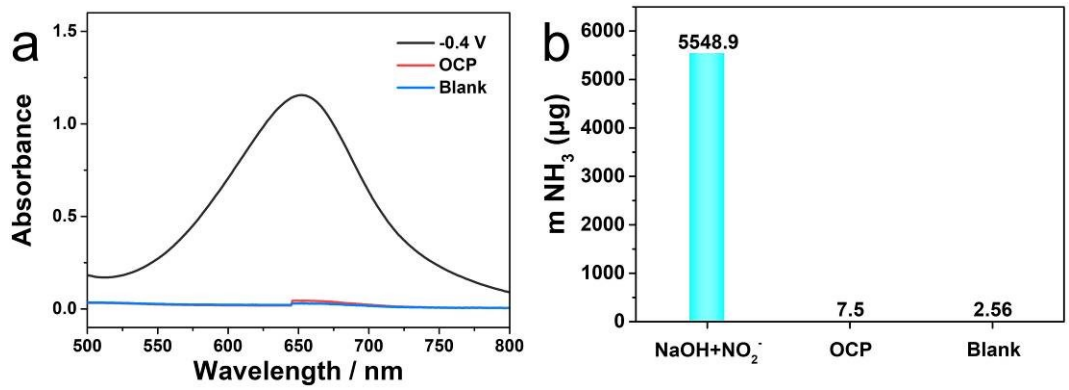

Fig. S11. (a) UV−Vis spectra and (b) amounts of electrogenerated NH_3 under different operating conditions.

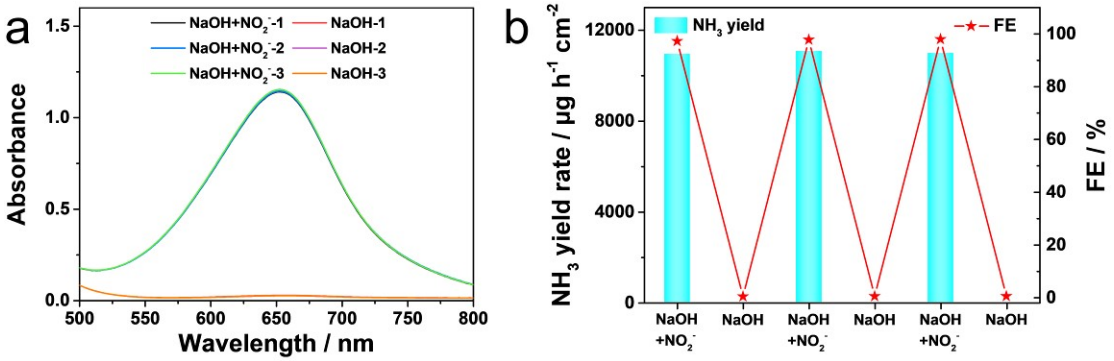

Fig. S12. (a) UV−Vis spectra and (b) amounts of electrogenerated NH_3 at -0.4V.

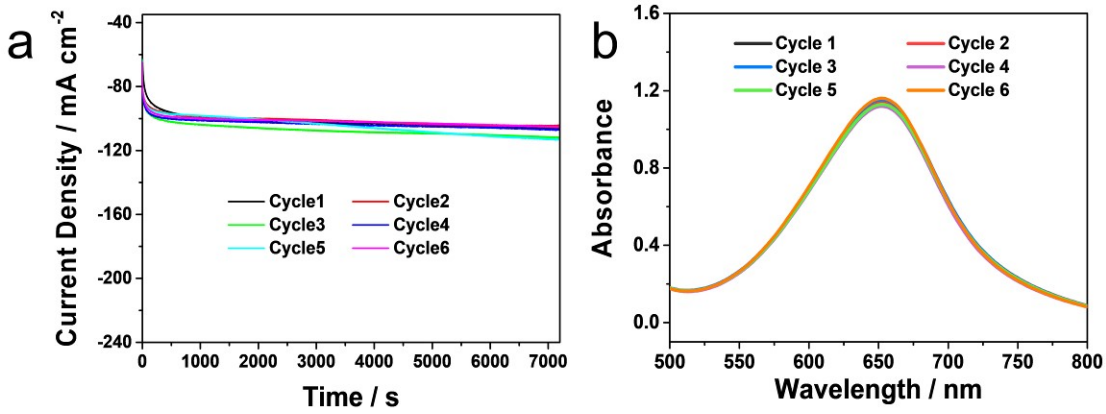

Fig. S13. (a) Chronoamperometry curves and (b) corresponding UV−Vis absorption spectra of C-$NiWO_4$/NF for electrochemical catalytic production of NH_3 during cycling tests in 0.1 M NaOH with 0.1 M NO_2^- at −0.4 V.

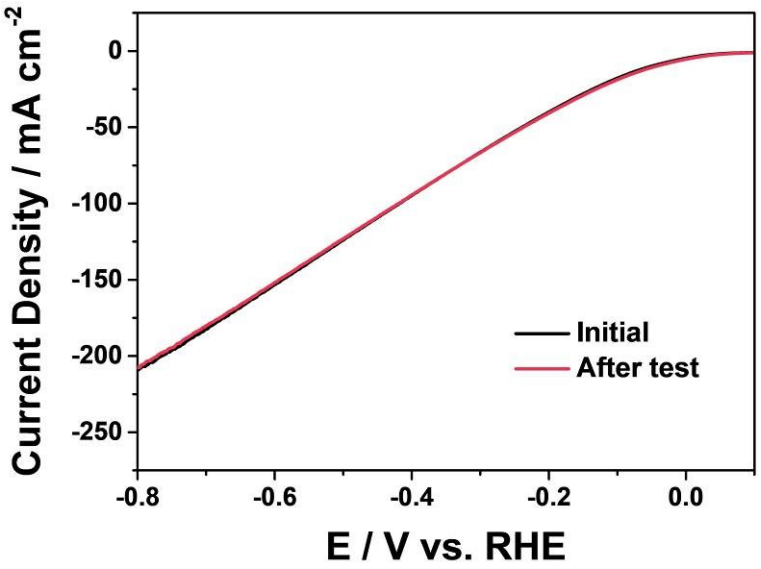

Fig. S14. LSV curves before and after the stability test.

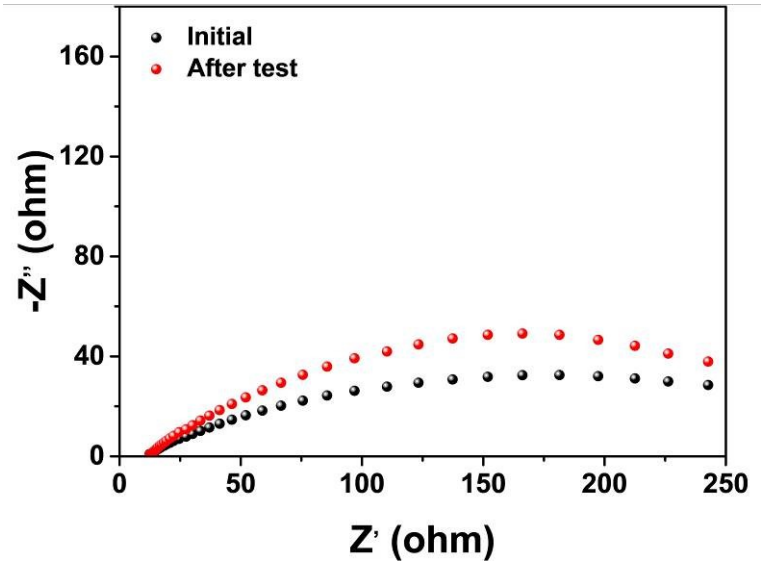

Fig. S15. EIS before and after the stability test.

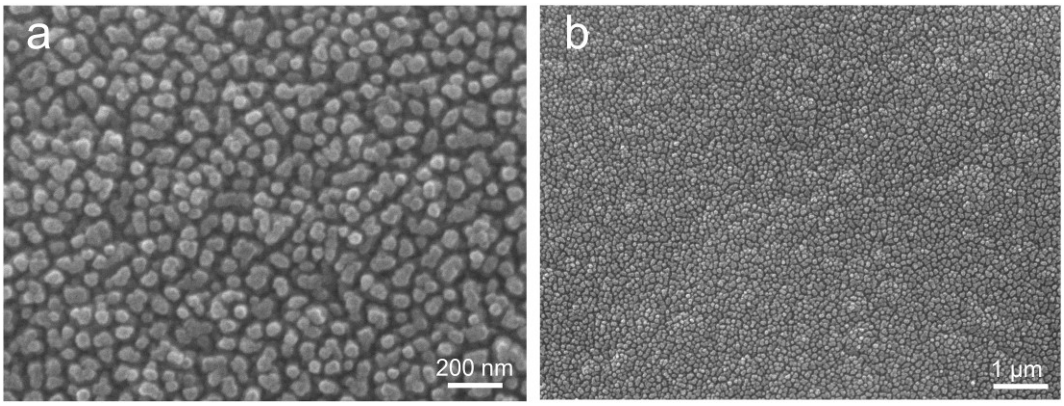

Fig. S16. SEM images of C-$NiWO_4$/NF after long-term electrolysis.

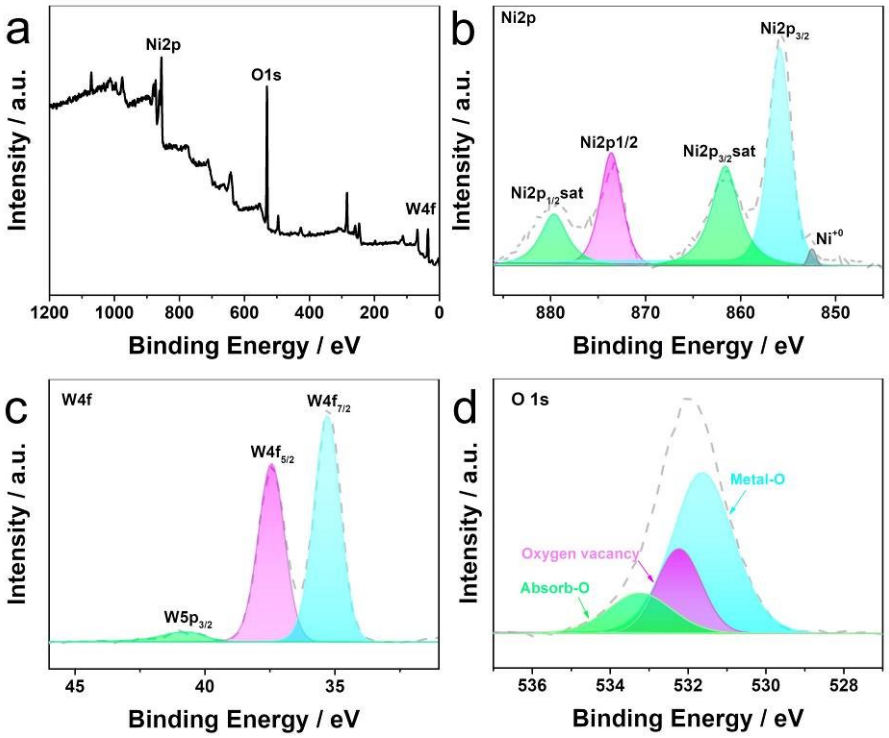

Fig. S17. (a) XPS survey spectrum. High-resolution XPS spectra of Ni 2p (b), W 4f (c), and O 1s (d) of C-$NiWO_4$/NF after long-term electrolysis.

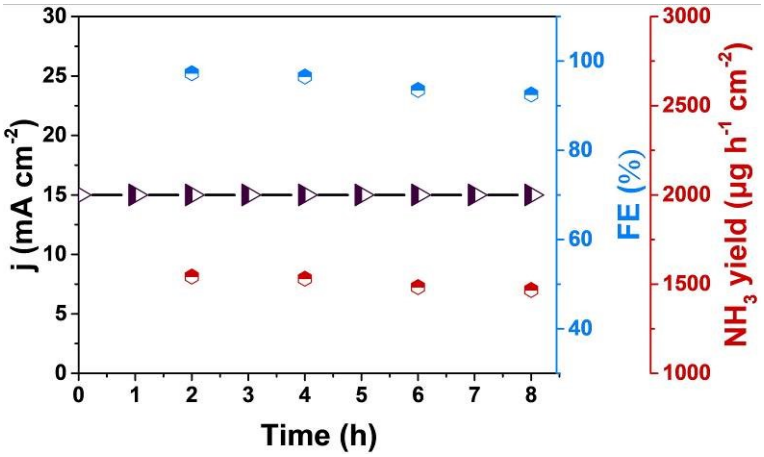

Fig. S18. Long-term NO_2^-RR experiment and corresponding NH_3 yields and FEs with C-$NiWO_4$/NF battery system at 15 mA cm^{-2}.

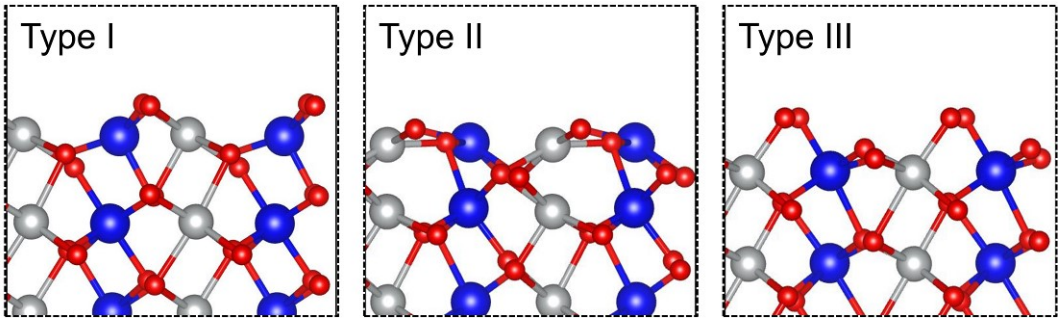

Fig. S19. Atomic configurations of $NiWO_4$(002) with different terminated faces.

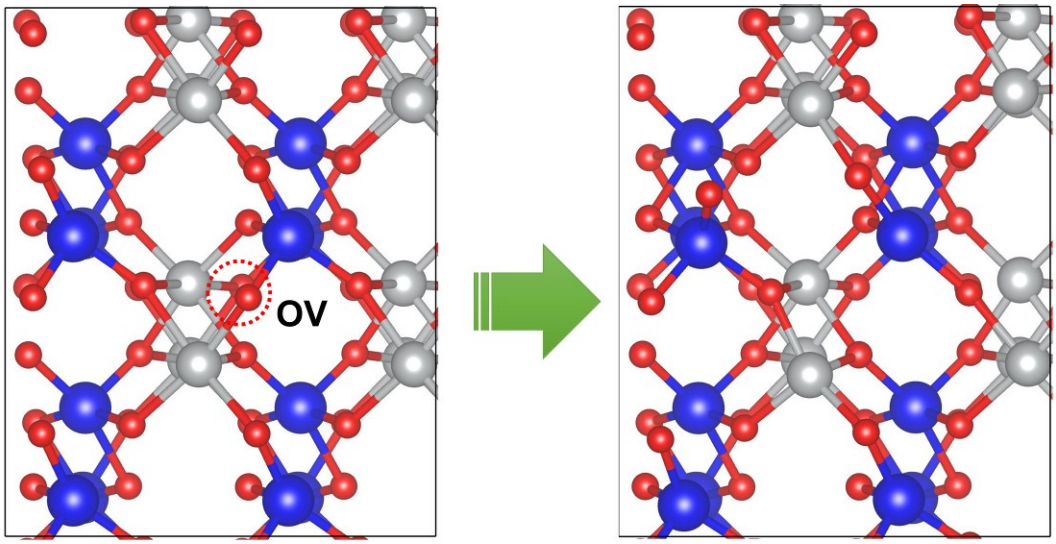

Fig. S20. Atomic configurations of $NiWO_4$-x(002).

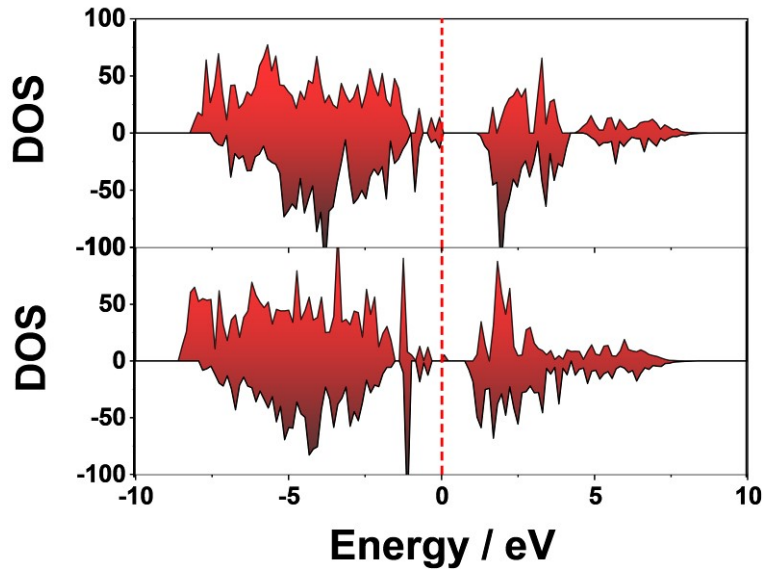

Fig. S21. DOS of $NiWO_4$(002) (up) and $NiWO_{4-x}$(002) (down), respectively.

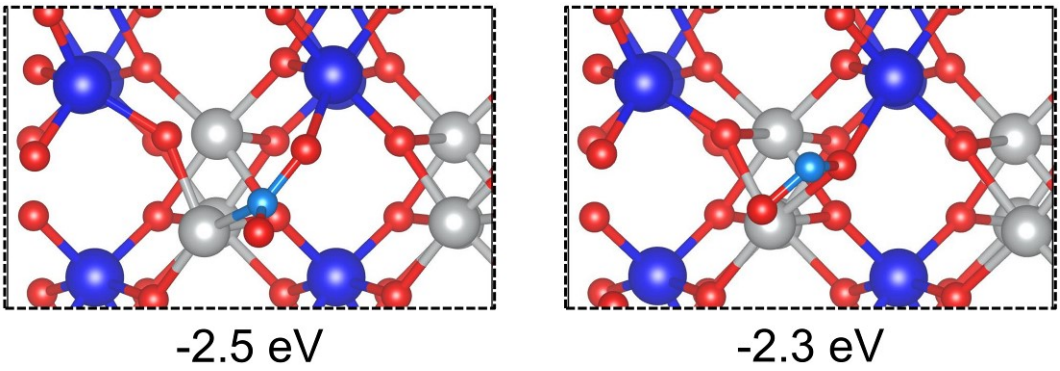

Fig. S22. Atomic configurations of NO_2^- adsorption on $NiWO_{4-x}$(002) face.

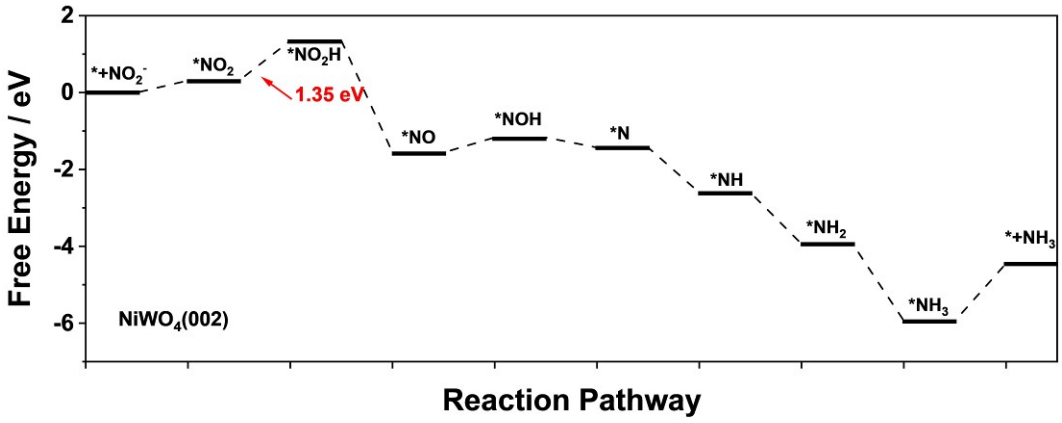

Fig. S23. Free energy diagram of NO_2^-RR on $NiWO_4$(002).

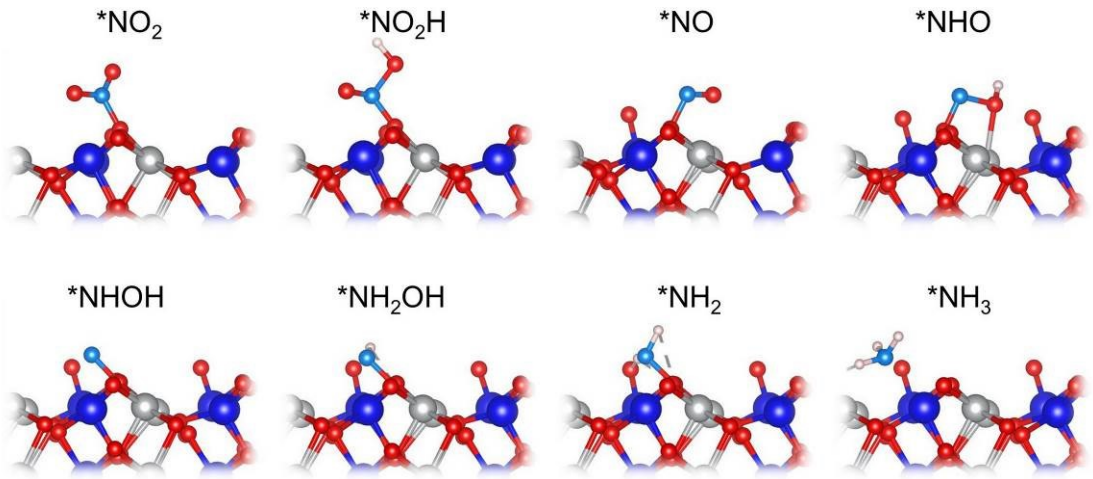

Fig. S24. Atomic configurations of NO_2^-RR on $NiWO_4$(002).

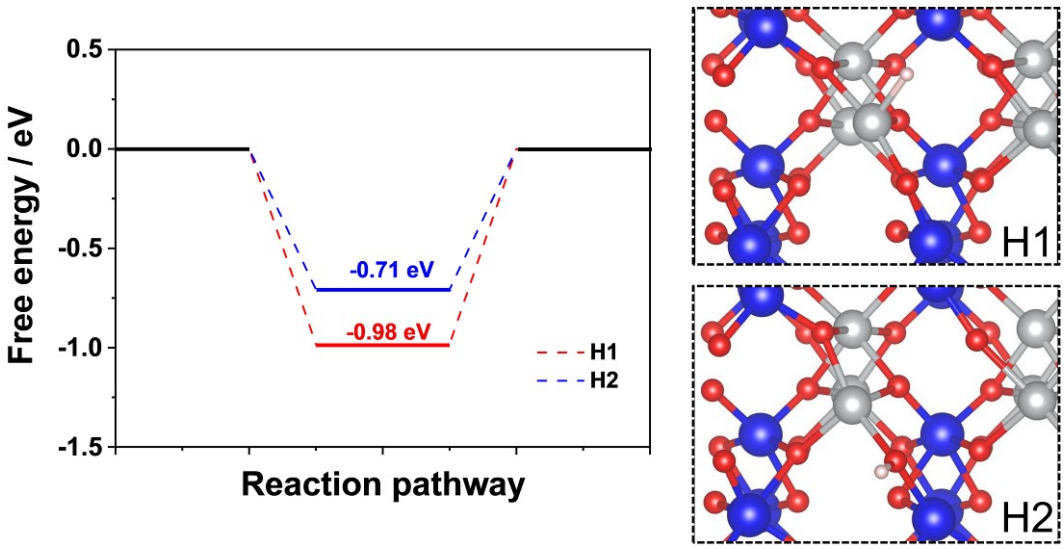

Fig. S25. Free energy diagram and corresponding atomic configurations of HER on the $NiWO_{4-x}$(002) surface.

Table S1. Comparison of catalytic performance of C-$NiWO_4$/NF with other reported NO_2^-RR electrocatalysts.

Catalyst	Electrolyte	FE (%)	NH_3 yield rate	Refs.
C-$NiWO_4$/NF	**0.1 M NaOH (0.1 M $NaNO_2$)**	**97.6**	**10974.36 μg h^{-1} cm^{-2} (645.55 μmol cm^{-2})**	**This work**
WO_2/WP	0.1 M NaOH (0.1 M $NaNO_2$)	94.32	880.25μmol cm^{-2} h^{-1}	7
CF@Cu_2O	0.1 M PBS (0.1 M $NaNO_2$)	94.2	441.8 μmol cm^{-2} h^{-1}	8
$[Co(DIM)Br_2]^+$	0.1 M $NaNO_2$	88	—	9
Oxo-MoS_x	0.1 M nitrite in 0.2 M citric acid (pH = 5)	13.5	—	10
$Cu_{80}Ni_{20}$	20 mM $NaNO_2$ (1.0 M NaOH)	87.6	—	11
Cu phthalocyanine	$NaNO_2$ (0.1 M KOH)	78	—	12
MnO_2 nanoarrays	0.1M Na_2SO_4 (4 mM $NaNO_2$)	6.0	3.09 × 10–11 mol s^{-1} cm^{-2}	13
Rh/Al_2O_3	25 mM phosphate Buffer+50 mM NO_2^-	68~95	—	14
Ni−NSA−V_{Ni}	0.2 M Na_2SO_4 (200 ppm NO_2^-)	88.9	235.98 μmol h^{-1} cm^{-2}	15
Cobalt-tripeptide complex	1.0 M MOPS buffer (1.0 M $NaNO_2$)	90±3	3.01 × 10^{-10} mol s^{-1} cm^{-2}	16
Poly-NiTRP complex	$NaNO_2$ (0.1 M $NaClO_4$)	—	1.1 mM	17
FeN_5H_2	1.0 M MOPS (1.0 M $NaNO_2$)	> 90	—	18
Cu_3P NA/CF	0.1 M PBS (0.1 M $NaNO_2$)	91.2 ± 2.5	1626.6 μg h^{-1} cm^{-2}	19

Table S2. Comparison of NH_3 yield and power density of our battery with recent Zn-N_2, Zn-NO, Zn-NO_2^-, or Zn-NO_3^- battery systems.

Catalyst	Battery Type	Power density (mW cm^{-2})	Refs.
C-$NiWO_4$/NF	**Zn-NO_2^-**	**5.55**	**This work**
Cu NDs	Zn-N_2	0.0101	20
FeHTNs	Zn-N_2	0.01642	21
VN@NSC	Zn-N_2	0.01642	22
CoPi/HSNPC	Zn-N_2	0.31	23
NbS_2	Zn-N_2	0.31	24
CoPi/NPCS	Zn-N_2	0.49	25
Ti_2O_3	Zn-N_2	1.02	26
$FePS_3$	Zn-N_2	2.6	27
CoP	Zn-NO	0.496	28
NiO	Zn-NO	0.88	29
MoS_2	Zn-NO	1.04	30
Fe_2O_3	Zn-NO	1.18	31
Ni_2P	Zn-NO	1.53	32
TiO_2@Ti	Zn-NO	1.7	33
MoC	Zn-NO	1.8	34
VN	Zn-NO	2.0	35
CoS	Zn-NO	2.06	36
BiNDs	Zn-NO	2.33	37
Bi@C	Zn-NO	2.35	38
ITO@TiO_2TP	Zn-NO_2^-	1.22	39
A-TiO_{2-x}	Zn-NO_2^-	2.38	40
TiO_2	Zn-NO_3^-	0.87	41
Fe/Ni_2P	Zn-NO_3^-	3.25	42
Co_2AlO_4	Zn-NO_3^-	3.43	43
CeO_2	Zn-NO_3^-	3.44	44
$NiCo_2O_4$	Zn-NO_3^-	3.94	45

References

1 G. Kresse, J. Hafner, Phys. Rev. B 1993, 47, R558–R561.

2 G. Kresse, J. Hafner, Phys. Rev. B, 49 (1994) 14251–14269.

3 J.P. Perdew, K. Burke, M. Ernzerhof, Phys. Rev. Lett., 77 (1996) 3865–3868.

4 G. Kresse, D. Joubert, Phys. Rev. B, 59 (1999) 1758–1775.

5 S. Ehrlich, J. Moellmann, W. Reckien, T. Bredow, S. Grimme, ChemPhysChem, 12(2011), 3414–3420.

6 N. Doudin, S. Pomp, M. Blatnik, R. Resel, M. Vorokhta, J. Goniakowski, C. Noguera, F.P. Netzera, Surface Science, 659 (2017) 20–30.

7 H. Qiu, Q. Chen, X. An, Q. Liu, L. Xie, J. Zhang, W. Yao, Y. Luo, S. Sun and Q. Kong, WO_2 nanoparticles with oxygen vacancies: a high-efficiency electrocatalyst for the conversion of nitrite to ammonia, J. Mater. Chem. A, 2022, 10, 24969-24974.

8 Q. Chen, X. An, Q. Liu, X. Wu, L. Xie, J. Zhang, W. Yao, M. S. Hamdy, Q. Kong and X. Sun, *Chem. Commun.*, 2022, **58**, 517-520.

9 S. Xu, H.-Y. Kwon, D. C. Ashley, C.-H. Chen, E. Jakubikova and J. M. Smith, *Inorg. Chem.*, 2019, **58**, 9443-9451.

10 D. He, Y. Li, H. Ooka, Y. K. Go, F. Jin, S. H. Kim and R. Nakamura, *J. Am. Chem. Soc.*, 2018, **140**, 2012-2015.

11 L. Mattarozzi, S. Cattarin, N. Comisso, P. Guerriero, M. Musiani, L. Vázquez-Gómez and E. Verlato, *Electrochim. Acta*, 2013, **89**, 488-496.

12 N. Chebotareva and T. Nyokong, *J. Appl. Electrochem.*, 1997, **27**, 975-981.

13 R. Wang, Z. Wang, X. Xiang, R. Zhang, X. Shi and X. Sun, *Chem. Commun.*, 2018, **54**, 10340-10342.

14 C. A. Clark, C. P. Reddy, H. Xu, K. N. Heck, G. Luo, T. P. Senftle and M. S. Wong, *ACS Catal.*, 2019, **10**, 494-509.

15 C. Wang, W. Zhou, Z. Sun, Y. Wang, B. Zhang and Y. Yu, *J. Mater. Chem. A*, 2021, **9**, 239-243.

16 Y. Guo, J. R. Stroka, B. Kandemir, C. E. Dickerson and K. L. Bren, *J. Am. Chem. Soc.*, 2018, **140**, 16888-16892.

17 P. Dreyse, M. Isaacs, K. Calfumán, C. Cáceres, A. Aliaga, M. J. Aguirre and D. Villagra, *Electrochim. Acta*, 2011, **56**, 5230-5237.

18 J. R. Stroka, B. Kandemir, E. M. Matson and K. L. Bren, *ACS Catal.*, 2020, **10**, 13968-13972.

19 J. Liang, B. Deng, Q. Liu, G. Wen, Q. Liu, T. Li, Y. Luo, A. A. Alshehri, K. A. Alzahrani and D. Ma, *Green Chem.*, 2021, **23**, 5487-5493.

20 C. Du, Y. Gao, J. Wang and W. *Chem. Commun.*, 2019, **55**, 12801-12804.

21 X.-W. Lv, X.-L. Liu, L.-J. Gao, Y.-P. Liu and Z.-Y. Yuan, *J. Mater. Chem. A*, 2021, **9**, 4026-4035.

22 X.-W. Lv, Y. Liu, Y.-S. Wang, X.-L. Liu and Z.-Y. Yuan, *Appl. Catal. B*, 2021, **280**, 119434.

23 J.-T. Ren, L. Chen, Y. Liu and Z.-Y. Yuan, *J. Mater. Chem. A*, 2021, **9**, 11370-11380.

24 H. Wang, J. Si, T. Zhang, Y. Li, B. Yang, Z. Li, J. Chen, Z. Wen, C. Yuan, L.

Lei and Y. Hou, *Appl. Catal. B*, 2020, **270**, 118892.

25 J. T. Ren, L. Chen, H. Y. Wang and Z. Y. Yuan, *ACS Appl. Mater. Interfaces*, 2021, **13**, 12106-12117.

26 H.-j. Chen, Z.-q. Xu, S. Sun, Y. Luo, Q. Liu, M. S. Hamdy, Z.-s. Feng, X. Sun and Y. Wang, *Inorg. Chem. Front.*, 2022, **9**, 4608-4613.

27 H. Wang, Z. Li, Y. Li, B. Yang, J. Chen, L. Lei, S. Wang and Y. Hou, *Nano Energy*, 2021, **81**.

28 J. Liang, W.-F. Hu, B. Song, T. Mou, L. Zhang, Y. Luo, Q. Liu, A. A. Alshehri, M. S. Hamdy, L.-M. Yang and X. Sun, *Inorg. Chem. Front.*, 2022, **9**, 1366-1372.

29 P. Liu, J. Liang, J. Wang, L. Zhang, J. Li, L. Yue, Y. Ren, T. Li, Y. Luo, N. Li, B. Tang, Q. Liu, A. M. Asiri, Q. Kong and X. Sun, *Chem. Commun.*, 2021, **57**, 13562-13565.

30 L. Zhang, J. Liang, Y. Wang, T. Mou, Y. Lin, L. Yue, T. Li, Q. Liu, Y. Luo, N. Li, B. Tang, Y. Liu, S. Gao, A. A. Alshehri, X. Guo, D. Ma and X. Sun, *Angew. Chem. Int. Ed*, 2021, **60**, 25263-25268.

31 J. Liang, H. Chen, T. Mou, L. Zhang, Y. Lin, L. Yue, Y. Luo, Q. Liu, N. Li, A. A. Alshehri, I. Shakir, P. O. Agboola, Y. Wang, B. Tang, D. Ma and X. Sun, *J. Mater. Chem. A*, 2022, **10**, 6454-6462.

32 T. Mou, J. Liang, Z. Ma, L. Zhang, Y. Lin, T. Li, Q. Liu, Y. Luo, Y. Liu, S. Gao, H. Zhao, A. M. Asiri, D. Ma and X. Sun, *J. Mater. Chem. A*, 2021, **9**, 24268-24275.

33 J. Liang, P. Liu, Q. Li, T. Li, L. Yue, Y. Luo, Q. Liu, N. Li, B. Tang, A. A. Alshehri, I. Shakir, P. O. Agboola, C. Sun and X. Sun, *Angew. Chem. Int. Ed*, 2022, **61**, e202202087.

34 G. Meng, M. Jin, T. Wei, Q. Liu, S. Zhang, X. Peng, J. Luo and X. Liu, *Nano Res.*, 2022, DOI: 10.1007/s12274-022-4747-y.

35 D. Qi, F. Lv, T. Wei, M. Jin, G. Meng, S. Zhang, Q. Liu, W. Liu, D. Ma, M. S. Hamdy, J. Luo and X. Liu, *Nano Res. Energy*, 2022, **1,** e9120022.

36 L. Zhang, Q. Zhou, J. Liang, L. Yue, T. Li, Y. Luo, Q. Liu, N. Li, B. Tang, F. Gong, X. Guo and X. Sun, *Inorg. Chem.*, 2022, **61**, 8096-8102.

37 Y. Lin, J. Liang, H. Li, L. Zhang, T. Mou, T. Li, L. Yue, Y. Ji, Q. Liu, Y. Luo, N. Li, B. Tang, Q. Wu, M. S. Hamdy, D. Ma and X. Sun, *Mater. Today Phys.*, 2022, **22**.

38 Q. Liu, Y. Lin, L. Yue, J. Liang, L. Zhang, T. Li, Y. Luo, M. Liu, J. You, A. A. Alshehri, Q. Kong and X. Sun, *Nano Res.*, 2022, **15**, 5032-5037.

39 S. Li, J. Liang, P. Wei, Q. Liu, L. Xie, Y. Luo and X. Sun, *eScience*, 2022, **2**, 382-388.

40 Z. Ren, Q. Chen, X. An, Q. Liu, L. Xie, J. Zhang, W. Yao, M. S. Hamdy, Q. Kong and X. Sun, *Inorg. Chem.*, 2022, **61**, 12895-12902.

41 Y. Guo, R. Zhang, S. Zhang, Y. Zhao, Q. Yang, Z. Huang, B. Dong and C. Zhi, *Energy Environ. Sci.*, 2021, **14**, 3938-3944.

42 R. Zhang, Y. Guo, S. Zhang, D. Chen, Y. Zhao, Z. Huang, L. Ma, P. Li, Q. Yang, G. Liang and C. Zhi, *Adv. Energy Mater.*, 2022, **12**.

43 Z. Deng, J. Liang, Q. Liu, C. Ma, L. Xie, L. Yue, Y. Ren, T. Li, Y. Luo, N. Li, B. Tang, A. Ali Alshehri, I. Shakir, P. O. Agboola, S. Yan, B. Zheng, J. Du, Q. Kong and X. Sun, *Chem. Eng. J.*, 2022, **435**.

44 Z. Li, Z. Deng, L. Ouyang, X. Fan, L. Zhang, S. Sun, Q. Liu, A. A. Alshehri, Y. Luo, Q. Kong and X. Sun, *Nano Res.*, 2022, DOI: 10.1007/s12274-022-4863-8.

45 Q. Liu, L. Xie, J. Liang, Y. Ren, Y. Wang, L. Zhang, L. Yue, T. Li, Y. Luo, N. Li, B. Tang, Y. Liu, S. Gao, A. A. Alshehri, I. Shakir, P. O. Agboola, Q. Kong, Q. Wang, D. Ma and X. Sun, *Small*, 2022, **18,** 2106961.